Numerical evidence of superuniversality of the two-dimensional and three-dimensional random quantum Potts models

Valentin Anfray● and Christophe Chatelain●

Université de Lorraine, CNRS, LPCT, F-54000 Nancy, France

The random q-state quantum Potts model is studied on hypercubic lattices in dimensions 2 and 3 using the numerical implementation of the strong disorder renormalization group introduced by Kovacs and Iglói [Phys. Rev. B **82**, 054437 (2010)]. Critical exponents ν, d_f, and ψ at the infinite disorder fixed point are estimated by finite-size scaling for several numbers of states q between 2 and 50. When scaling corrections are not taken into account, the estimates of both d_f and ψ systematically increase with q. It is shown, however, that q-dependent scaling corrections are present and that the exponents are compatible within error bars, or close to each other, when these corrections are taken into account. This provides evidence of the existence of a superuniversality of all two- and three-dimensional random Potts models.

I. INTRODUCTION

Random quantum ferromagnets are known to undergo a very peculiar phase transition for which quantum fluctuations, which drive the transition in the absence of disorder, are dominated by disorder fluctuations. Thanks to this peculiarity, the properties of the infinite-disorder fixed point (IDFP) that governs the critical behavior at the transition can be studied using a rather simple real-space renormalization group, introduced by Ma and Dasgupta [1], referred to as a strong disorder renormalization group (SDRG). In the case of the random transverse-field Ising chain (RTIM), Fisher was able to find the asymptotic solution of the flow equations and determine the critical exponents exactly [2–5]. In particular, the dynamical exponent z is infinite at the fixed point, whereas $z = 1$ for the pure RTIM. The excitation gap ΔE displays an activated scaling corresponding to an essential singularity $\Delta E \sim e^{-aL^\psi}$ with lattice size L, where the critical exponent is $\psi = 1/2$. The average magnetization density follows a power law $m \sim L^{d_f - d}$ with a fractal dimension $d_f = d - \phi\psi$ and a magnetic critical exponent ϕ equal to the golden number $(1 + \sqrt{5})/2$. These exponents are expected to be exact. Away from the critical point, in the so-called Griffiths phases, the dynamics is dominated by rare macroscopic clusters of strong (resp. weak) couplings that are ordered (resp. disordered) while the rest of the system is in the disordered (resp. ordered) phase [6]. As a consequence, the dynamical exponent is larger than 1 and diverges with the control parameter δ as $1/|\delta|$ as the IDFP is approached [7]. Finally, the correlation length diverges as $\xi \sim |\delta|^{-\nu}$ with $\nu = 2$ for the average spin-spin correlations, while it is $\nu = 1$ for the typical ones.

The universality class of the RTIM turned out to be quite robust: the number of states q of the 1D random quantum Potts model was shown to be an irrelevant parameter in the SDRG flow equations [8]. Therefore the critical behavior is described by the same IDFP as the RTIM for all values of

the number of states q, in contrast to what is observed in the classical case where the magnetic critical exponent increases smoothly with q [9–12]. For a sufficiently strong disorder, the critical behavior of the random q-state quantum clock model is also expected to be governed by the same IDFP as the RTIM [8,13]. The random contact process, whose SDRG flow equations are identical to those of the RTIM, also belongs to the universality class of the RTIM [14–16]. The random quantum N-color Ashkin-Teller chain, equivalent to N coupled Ising chains, has attracted much attention in the last decade. In the case $N = 2$, the phase diagram is qualitatively unchanged by the introduction of disorder [13]. Along the self-dual transition line, the interchain coupling is an irrelevant parameter in the SDRG flow equations [17]. As a consequence, the critical behavior is again the same as for the random RTIM, whereas exponents vary along the line in the pure case. For strong interchain coupling, the transition line splits into two lines, enclosing a new intermediate phase acting as a double-Griffiths phase [18,19]. Despite the fact that the interchain coupling flows towards an infinite value during renormalization, the critical behavior is still in the RTIM universality class along these two lines [18]. In the case $N \geqslant 3$, the pure Ashkin-Teller chain undergoes a first-order phase transition, as in the Potts model with $q \geqslant 4$, which becomes continuous in presence of disorder [17,20–23]. The critical behavior is in the RTIM universality class at weak interchain coupling but seems to be governed by a distinct IDFP at stronger interchain coupling [21].

In this paper we address the question of whether the robustness of the universality class of the RTIM is specific to the one-dimensional (1D) case or exists also in higher dimensions. Much less is known about two- or three-dimensional (2D, 3D) random quantum ferromagnets. The extension of the SDRG to higher dimensions is trivial, but the flow equations are then too complicated for an analytical solution to be found. The numerical implementation of the SDRG rules is

complicated by the fact that the topology of the lattice changes during the renormalization. A single site, or cluster, is coupled to a large number of other spins after only a few iterations. Nevertheless, the critical behavior of the 2D RTIM could be shown to be governed by an IDFP [24]. An efficient algorithm, allowing for accurate estimates of the critical exponents, was introduced by Kovacs and Iglói [25–27]. They were able to show that the critical exponents of the random RTIM depend on the dimension of the lattice. Recently, the critical behavior of the 2D quantum Potts model with a quasiperiodic modulation of the couplings was shown to be governed by an infinite quasiperiodicity fixed point, distinct from an IDFP but with an infinite dynamical exponent like an IDFP [28,29]. Interestingly, the critical exponents are compatible within error bars for all numbers of states $q \geqslant 3$. Later on, Kang *et al.* discussed the IDFP of the random quantum Potts model in light of a mapping onto a discrete gauge model, where the size of the gauge group is equal to the number of states q of the Potts model [30]. Quantum Monte Carlo simulations were performed for the two-dimensional random quantum Ising model and the three-state Potts model. The numerical estimates of the critical exponents of the two models are in good agreement, providing evidence of an independence on q and the superuniversality of the IDFP in two dimensions.

In this work, the q-state random quantum Potts model is considered in two and three dimensions. Since in the classical 2D random Potts model, the magnetic critical exponent increases slowly with q, we considered number of states up to $q = 50$. Critical exponents are estimated numerically using the Kovacs-Iglói algorithm. In the first section of this paper, the model and the algorithm are presented. The determination of the location of the critical points is detailed in Sec. III. The correlation length exponent ν is extracted from the statistics of the pseudocritical points. In Sec. IV, the magnetic fractal dimension d_f is estimated from the finite-size scaling of the average magnetic moment. In Sec. V, the exponent ψ is estimated from the analysis of the average energy gap. Conclusions follow.

II. POTTS MODEL AND SDRG ALGORITHM

A. The random quantum Potts model

The q-state quantum Potts model is defined on a lattice $\Lambda = (V, E)$ by the Hamiltonian [31,32]

$$H_{\text{Potts}} = -\sum_{(i,j)\in E} J_{ij} D_{i,j} - \frac{1}{q} \sum_{i \in V} h_i M_i \qquad (1)$$

acting on the Hilbert space spanned by the states $\bigotimes_{i \in V} |n_i\rangle$ with $n_i = 0, \ldots, q-1$. The first sum extends over the set E of edges of the lattice Λ, and the matrix elements of the diagonal operator $D_{i,j}$ vanish unless $n_i = n_j$, in which case they are equal to 1. A representation of this operator in terms of local operators is given by

$$D_{i,j} = \frac{1}{q} \sum_{n=0}^{q-1} \Omega_i^n \Omega_j^{-n}, \qquad (2)$$

where $\Omega_i = \mathbb{1}^{\otimes i-1} \otimes \Omega \otimes \mathbb{1}^{\otimes N-i}$ (N is the number of sites of the lattice) and Ω is a diagonal $q \times q$ matrix whose diagonal

elements are ω^n with $\omega = e^{2i\pi/q}$. In the pure case, i.e., $J_{ij} = J > 0$, the first term of the Hamiltonian favors a ferromagnetic ordering of the spins, i.e., $n_i = n$ $\forall i$. The second sum of the Hamiltonian (1) extends over the set V of sites of the lattice Λ and $M_i = \mathbb{1}^{\otimes i-1} \otimes M \otimes \mathbb{1}^{\otimes N-i}$, with M the $q \times q$ matrix whose elements are all equal to 1. In the pure case, $h_i = h$, the second term of the Hamiltonian destroys the ferromagnetic ordering and is associated to quantum fluctuations. When $q = 2$, the Potts model is equivalent to the RTIM, whose Hamiltonian takes the simpler form

$$H_{\text{Ising}} = -\sum_{(i,j)\in E} J_{ij}\sigma_i^z \sigma_j^z - \sum_{i \in V} h_i \sigma_i^x, \qquad (3)$$

where $\sigma_i^{x,z}$ are Pauli matrices acting on site i of the lattice. In the one-dimensional case, only the Ising model is exactly solvable when $J_{ij} = J$ and $h_i = h$. Duality arguments predict that the transition point is located at $J = h$ for any number of states q. The pure Potts chain undergoes a second-order phase transition when $q \leqslant q_c(1) = 4$ and a first-order transition when $q > q_c(1)$. At higher dimensions $d > 1$, the transition point is not known exactly. The number of states $q_c(d)$ separating the regime of the first- and second-order phase transition is also not known exactly for $d > 1$.

In the following, the Potts model with quenched disorder is considered. The exchange couplings J_{ij} and the transverse fields h_i are independent random variables distributed according to the distributions $P_0(J_{ij})$ and $Q_0(h_i)$. As mentioned in the Introduction, the critical exponents of the random RTIM ($q = 2$) has been determined exactly by Fisher. In dimensions $d = 2, 3$, and 4, they were estimated numerically by Kovacs and Iglói. In the following, the RTIM will be used as a test bed for our implementation of the SDRG algorithm and for the analysis of the numerical data. In the regime $q > q_c(d)$, the first-order phase transition of the pure Potts model is expected to be rounded by disorder and turned into a continuous transition, as first discussed by Goswami *et al.* [17]. A rigorous proof was later given that an infinitesimal amount of disorder is sufficient to round any first-order phase transitions in quantum systems in dimensions $d \leqslant 2$ [33,34]. For $d > 2$, the first-order phase transition may survive at weak disorder, as in the classical case for $d \geqslant 3$, for example, in the random 3D four-state classical Potts model [35,36].

In this work, several probability distributions were considered. The uniform distribution

$$P_0(J_{ij}) = \Theta(J_{ij})\Theta(1 - J_{ij}), \qquad (4)$$

where Θ is the Heaviside function for the exchange couplings and

$$Q_0(h_i) = \frac{1}{h_{\max}} \Theta(h_i)\Theta(h_{\max} - h_i) \qquad (5)$$

for the transverse fields. The Potts model is in the ferromagnetic phase for a sufficiently small parameter $\theta = \log h_{\max}$ and in the paramagnetic phase for large θ. The distributions (4) and (5) are referred to as weak disorder in the following. These distributions are expected to evolve along the renormalization group (RG) flow and become broader and broader. Because the distributions P_0 and Q_0 are far from the distributions at the IDFP, corrections to scaling are expected for small lattice

sizes and therefore small numbers of RG steps. To minimize these corrections, power-law distributions

$$P_0(J_{ij}) \sim J_{ij}^{-\Delta}, \quad (0 < J_{ij} < 1)$$
$$Q_0(h_i) \sim h_i^{-\Delta}, \quad (0 < h_i < h_{\max}) \tag{6}$$

were also considered for several numbers of states q of the Potts model. The value $\Delta = 2/3$ is referred to as a medium disorder and $\Delta = 4/5$ as a strong disorder.

B. SDRG algorithm

The strong disorder renormalization group is a real-space decimation scheme where the strongest coupling $\Omega = \max(\{J_{ij}\}, \{h_i\})$ is decimated at each iteration [2–4]. The case of the RTIM is discussed first. If the strongest coupling is an exchange coupling, say $\Omega = J_{ij}$, the two spins i and j are merged into a new effective cluster whose magnetic moment $\mu' = \mu_i + \mu_j$ is the sum of the moments μ_i and μ_j of the two spins i and j. Second-order perturbation theory shows that this new cluster is coupled to an effective transverse field $h' = \frac{h_i h_j}{J_{ij}}$ and to any other spin $k \neq i, j$ by an exchange coupling $J'_{ik} = J_{ik} + J_{jk}$. If the strongest coupling Ω is a transverse field, say h_i, the spin i is decimated. An effective coupling is induced between all pairs of spins k and l that were both coupled to site i. To second order in perturbation theory, this effective coupling is $J'_{kl} = J_{kl} + \frac{J_{ik}J_{il}}{h_i}$. As this scheme is iterated, the probability distributions $P(J)$ and $Q(h)$ of the couplings become broader and broader so that second-order perturbation theory is expected to become exact at the IDFP. The sum rule can then be replaced by a maximum rule: at the IDFP, it is sufficient to write the exchange coupling of a spin k with the new effective cluster at site i as the maximum $J'_{ik} = \max(J_{ik}, J_{jk})$ instead of the sum. Similarly, the effective exchange coupling J'_{kl} induced by the decimation of the site i can be simplified as $J'_{kl} = \max(J_{kl}, \frac{J_{ik}J_{il}}{h_i})$. For the Potts model, the SDRG rules are shown to be [8]

$$h' = \frac{h_i h_j}{\kappa J_{ij}}, \quad J'_{kl} = J_{kl} + \frac{J_{ik}J_{il}}{\kappa h_i} \tag{7}$$

where $\kappa = q/2$. These rules are the same for any dimension d of the lattice. However, the main difficulty in implementing them numerically when $d > 1$ comes from the increasing number of couplings J_{ij} that are generated at each decimation. Finding the largest coupling requires more and more CPU time, and even storing all the couplings restricts the application to small lattice sizes. A crucial simplification was introduced by Kovács and Iglói [25–27]. They showed that many couplings are actually irrelevant at the IDFP. The resulting algorithm and the details of our implementation for the Potts model are discussed in the following.

The Hamiltonian can be seen as a weighted graph. A weight

$$r_i = -\ln h_i \tag{8}$$

is attached to each node i, and an edge with a distance

$$d_{ij} = d_{ji} = -\ln J_{ij} \tag{9}$$

is defined between each pair (i, j) of nodes of the graph for which $J_{ij} \neq 0$. With the above definitions, the SDRG rules become the following:

(a) If r_i is the global minimum, equivalently, if h_i is the global maximum, then the node i is removed. For all pairs of sites (k, l) connected to i, i.e., such that $J_{ik}, J_{il} \neq 0$, the distance d_{kl} is updated as

$$d'_{kl} = \min(d_{kl}, d_{ki} + d_{il} - r_i + \ln \kappa), \tag{10}$$

which is equivalent to (7) when replacing the sum rule by the maximum rule.

(b) If d_{ij} is the global minimum, or equivalently, if J_{ij} is the global maximum, then the two nodes i and j are merged into a single node i, whose weight is

$$r'_i = r_i + r_j - d_{ij} + \ln \kappa, \tag{11}$$

which is again equivalent to (7). For each node k previously connected to both i and j, i.e., $J_{ik}, J_{jk} \neq 0$, the distance to the new site i is updated as $d'_{ki} = \min(d_{ik}, d_{jk})$.

Several improvements can be implemented. First, instead of removing the node i when the spin is decimated ($\Omega = h_i$), it is set as inactive. The definition (9) of the distances d_{ij} is modified to

$$d_{ij} = d_{ji} = -\ln J_{ij} + \frac{l_i}{2}\ln(\kappa h_i) + \frac{l_j}{2}\ln(\kappa h_j), \tag{12}$$

where l_i is the activation status of the node i, which takes the value $l_i = 0$ when the node has not been decimated yet (the node is then said to be active) and 1 otherwise (the node is said to be inactive). By setting the node i as inactive instead of removing it when $\Omega = h_i$, it is not necessary anymore to add new edges associated to the effective couplings that are generated by second-order perturbation theory. Instead, the exchange coupling between two active sites k and l is computed *on the fly* when necessary as $J_{kl} = e^{-\delta_{kl}}$, where δ_{kl} is the shortest distance of all paths of the graph joining sites k and l and going through inactive sites only. If no path connects k and l, then $J_{kl} = 0$. The condition of the shortest distance is equivalent to the maximum rule and the SDRG rule is recovered. Indeed, when the site i is decimated, $\delta_{kl} = d_{ki} + d_{il} = -\ln J_{ki} + \ln(\kappa h_i) - \ln J_{il}$ so that the effective exchange coupling is $J'_{kl} = e^{-\delta_{kl}} = \frac{J_{ki}J_{il}}{\kappa h_i}$, as expected. The advantage of this implementation is that the number of edges does not grow during site decimation. Inactive sites are removed during edge decimation: if $\Omega = \delta_{ij}$, sites i and j are merged into a new cluster on site, say i. All inactive sites k belonging to the shortest path between sites i and j can now be removed, and all edges d_{kl} are added to d_{il} using the minimum rule $d'_{il} = \min(\delta_{il}, d_{ik} + d_{kl})$.

The computation of the shortest distance δ_{kl} between two sites can be time-consuming. Hopefully, the shortest distance can be determined efficiently using the Dijkstra algorithm [37]. Note that the Dijkstra algorithm requires the distances to be positive. The distance $d_{ij} = -\ln J_{ij}$ between two active sites can be made positive by initially choosing all exchange couplings J_{ij} smaller than or equal to 1. When $\kappa \geqslant 1$, the SDRG rules imply that $J'_{ij} \leqslant 1$ after renormalization. If the site j is inactive while i is active, the distance $d_{ij} = -\ln J_{ij} + \frac{1}{2}\ln(\kappa h_j)$ is positive, too, because the decimation of the node j has been possible only if $h_j > J_{ij}$. It fol-

lows that $-\ln J_{ij} + \frac{1}{2}\ln h_j + \frac{1}{2}\ln\kappa > -\frac{1}{2}\ln J_{ij} + \frac{1}{2}\ln\kappa \geqslant 0$, which completes the proof that $d_{ij} \geqslant 0$ when $\kappa \geqslant 1$ and $J_{ij} \leqslant 1$. However, the distance d_{ij} can be negative when the two sites are inactive. When this is the case, any path reaching site i will then go to site j. As a consequence, for any neighbor $k \neq i$ of site j, one can create or update the distance between i and k as $d'_{ik} = \min(d_{ik}, d_{ij} + d_{jk})$ and remove the site j and all edges d_{jk}.

The second improvement concerns the choice of the next coupling to be renormalized. It is not necessary to find the global minimum. Finding and decimating a local minimum is sufficient if the local minimum is defined as follows:

(i) r_i is a local minimum if $r_i < \delta_{ik}$ for all k such that there exists at least one path between i and k. No edge involving the node i can therefore be decimated before the node i.

(ii) δ_{ij} is a local minimum if $\delta_{ij} < r_i, r_j$ and if $\delta_{ij} < \delta_{ik}$ or $\delta_{ij} < \delta_{jk}$ when there exists at least one path between i or j and k.

These definitions ensure that a local minimum remains a local minimum when any another node or edge is decimated first. The proof follows from the following fact:

(i) If the node j is decimated first, which implies that $r_j < \delta_{jk}$ for all sites k for which there exists at least one path joining j and k, the site j is set inactive. The distances between the site j and its neighbors l are updated to $d'_{jl} = d_{jl} - \frac{1}{2}r_j + \frac{1}{2}\ln\kappa$. The shortest distance δ_{ik} is therefore unchanged if the shortest path does not go through the site j and becomes $\delta'_{ik} = \delta_{ij} + \delta_{jk} - r_j + \ln\kappa$ otherwise. Since $r_j < \delta_{jk}$ and $r_i < \delta_{ij}$ if r_i is a local minimum, the new value δ'_{ik} is necessarily larger than r_i. r_i remains therefore a local minimum.

(ii) If the edge δ_{jk} is decimated first, the distance between a site $i \neq j, k$ and the new site, say j, is updated to the value $\delta'_{ij} = \min(\delta_{ij}, \delta_{ik})$. If r_i is a local minimum, the condition $r_i < \delta_{ij}, \delta_{ik}$ holds. It follows that $r_i < \delta'_{ij}$ and therefore, r_i remains a local minimum.

Similarly, the distance δ_{ij} remains a local minimum in the following situations:

(i) If the node k is decimated first, which implies that $r_k < \delta_{kl}$, for all sites l for which there exists at least one path joining k and l, the shortest distance δ_{ij} is unchanged if the shortest path does not go through the site k and becomes $\delta'_{ij} = \delta_{ik} + \delta_{jk} - r_k + \ln\kappa$ otherwise. Since $r_k < \delta_{ik}, \delta_{jk}$ and $\delta_{ij} < \delta_{ik}$ or $\delta_{ij} < \delta_{jk}$ if δ_{ij} is a local minimum, the effective distance $\delta'_{ij} = \delta_{ik} + \delta_{jk} - r_k + \ln\kappa$ is larger than δ_{ij}. The latter will therefore remain a local minimum.

(ii) If the edge δ_{kl} is decimated first, the distance between a site $i \neq k, l$ and the new site, say k, is updated to the value $\delta'_{ik} = \min(\delta_{ik}, \delta_{il})$. If the δ_{ij} was a local minimum with the condition $\delta_{ij} < \delta_{ik}, \delta_{il}$, then $\delta_{ij} < \delta'_{ik}$ and therefore δ_{ij} remains a local minimum.

(iii) If the edge δ_{jk} is decimated first, the weight of the new node j becomes $r'_j = r_j + r_k - \delta_{jk} + \ln\kappa$. Since $\delta_{jk} < r_k$, the inequality $r'_j > r_j$ holds. Therefore if δ_{ij} is a local minimum, the condition $\delta_{ij} < r_j$ is preserved when the edge δ_{jk} is decimated. Distances will also be modified. In particular, δ_{ij} will be replaced by $\min(\delta_{ij}, \delta_{ik})$. Since δ_{jk} was decimated first, $\delta_{jk} < \delta_{ij}$, so the condition $\delta_{ij} < \delta_{il}$ for all l, for which there exists a path between i and l, should hold for δ_{ij} to be local minimum. In particular, $\delta_{ij} < \delta_{ik}$ and therefore the value of δ_{ij}
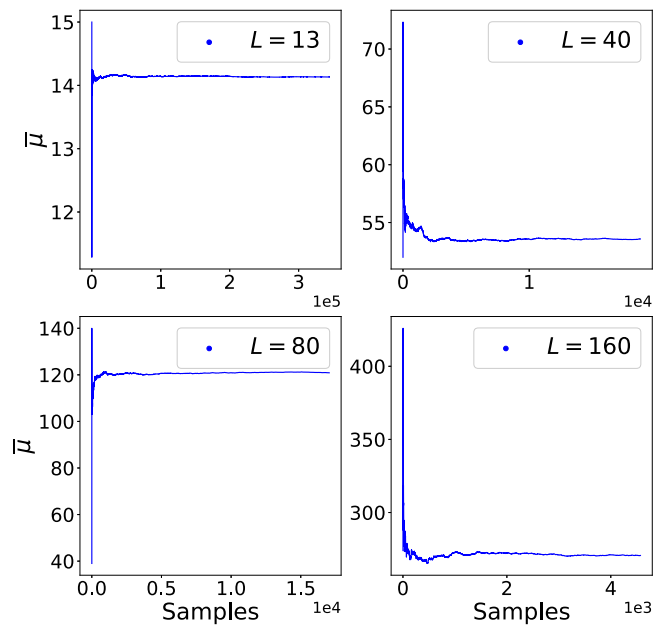

FIG. 1. Average value of the magnetic moment μ of the last decimated cluster of the 3D $q = 10$ Potts model with respect to the number of disordered samples. The four graphs correspond to different lattice sizes L. Note that the number of samples given on the x axis has to be multiplied by 10^5 ($L = 13$, top left), 10^4 ($L = 40$, top right), 10^4 ($L = 80$, bottom left), and 10^3 ($L = 160$, bottom right).

will not be modified by the decimation of δ_{jk}. For $l \neq k$, δ_{il} is unchanged because a path joining i and l can only go through inactive sites, so neither j or k. In conclusion, δ_{ij} will remain a local minimum after the decimation of δ_{jk}.

Local minimum can be decimated in any order. One can check that the same decimations as in the original SDRG will take place. Only the order differs. A lot of computation time is saved in looking for local minimum instead of the global one. The drawback of this method is that the renormalization flow being modified, one cannot study anymore the evolution of the total magnetic moment or the number of sites as a function of Ω. Instead, the critical exponents should be estimated from the behavior of the magnetic moment or the transverse field of the last decimated site in the original SDRG. In our implementation, this site could have been decimated anywhere in the RG flow, so one has to keep track of the smallest transverse field at each decimation.

III. CRITICAL POINT

The random q-state Potts model is studied on 2D and 3D hypercubic lattices with the above-detailed algorithm. The data have been averaged over more than 3000 disordered configurations for the largest lattice sizes and up to 10^6 for the smallest ones. These numbers were chosen in order to achieve a good convergence of average quantities. In Fig. 1 the average magnetic moment of the last decimated cluster during the original SDRG is plotted versus the number of samples in the case of the 3D ten-state Potts model. Rare events with a large contribution, usually expected in random systems, do not seem to have any influence on the plateau

reached by the average magnetic moment. As can be seen in Fig. 1 in the case of the 3D ten-state Potts model, the relative fluctuations of $\bar{\mu}$ are, in the worst case $L = 160$, of order $\frac{\Delta\mu}{\bar{\mu}} \simeq 1/150 < 1\%$. The estimation of the error as $\sqrt{\text{Var}\,\mu/N}$, where Var μ is the variance of the data and N the number of disordered configurations, leads to a relative error of 0.6% for the 3D ten-state Potts model at $L = 160$. For the critical exponents that will be estimated in the following, the error due to the finite number of disordered configurations is a small contribution compared to the error coming from the fits.

A pseudocritical point $\theta_c^i(L) \equiv \ln h_c^i(L)$ is determined for each disordered sample i using the doubling method [25,26]. Two identical replicas of the same system, i.e., with the same exchange couplings and transverse fields, are glued together with some specific boundary conditions. When the SDRG procedure is applied to both the joint system of size $2L$ and the initial one of size L, the ratio $\mu(2L)/\mu(L)$ of the magnetic moments of the last decimated cluster is expected to show a jump at the pseudocritical point. In the paramagnetic phase, $\theta > \theta_c^i(L)$, the decimated cluster is located in one of the two replicas and $\mu(2L) = \mu(L)$. In contrast, in the ferromagnetic phase, $\theta < \theta_c^i(L)$, the last decimated cluster spans the two replicas and $\mu(2L) = 2\mu(L)$. In practice, the system is considered to be in the ferromagnetic phase if the last decimated cluster contains the same sites in both replicas. To locate the pseudocritical point, an interval $[\theta_1, \theta_2]$ is manually chosen and is refined by performing additional simulations at $\theta = \frac{1}{2}(\theta_1 + \theta_2)$ until the targeted accuracy $\epsilon = |\theta_2 - \theta_1|$ is reached. In the following, the accuracy on the pseudocritical point $\theta_c^i(L)$ is 10^{-5}.

As the lattice size is increased, the pseudocritical points $\theta_c^i(L)$ are expected to converge to the critical point θ_c of the infinite system as

$$\left|\theta_c^i(L) - \theta_c\right| \sim L^{-1/\nu}, \tag{13}$$

where ν is the correlation length exponent. As a consequence, the probability distribution of the pseudocritical points $\theta_c^i(L)$ should be independent of the lattice size L when plotted with respect to the rescaled distance to the critical point $u = L^{1/\nu}|\theta_c^i(L) - \theta_c|/\theta_c$. This plot is shown in Fig. 2 for the 2D and 3D ten-state Potts models. As expected, all points fall nicely on the same curve when the two parameters θ_c and ν are appropriately chosen. To determine the values leading to the best collapse of the probability distributions $P_L(u)$ for different lattice sizes L, the following cost function,

$$\sigma = \frac{1}{u_{\max} - u_{\min}} \int_{u_{\min}}^{u_{\max}} \sum_L \left[P_L(u) - \frac{1}{N_L} \sum_L P_L(u) \right]^2 du, \tag{14}$$

was numerically minimized using the Powell method. Only $N_L = 4$ lattice sizes were considered. $u_{\min}$ and $u_{\max}$ are the smallest and largest values of u in the dataset. The optimal values of the parameters θ_c and ν are collected in Table I for the 2D and 3D Potts models. The estimates of the correlation length exponent ν are compatible within error bars for the 2D (resp. 3D) Potts model, independently of the number of states q of the Potts model.

The correlation length exponent ν was also estimated by performing a nonlinear fit of the shift of the average pseu-
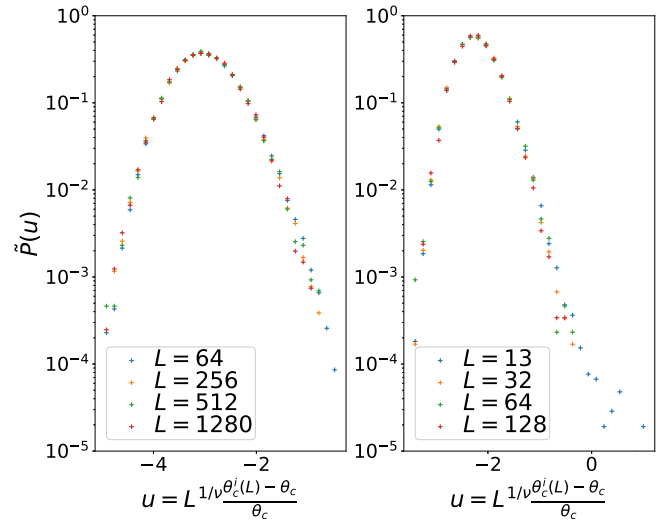

FIG. 2. Probability distribution $P(u)$ of the rescaled distance $u = L^{1/\nu}[\theta_c^i(L) - \theta_c]/\theta_c$ to the critical point for the four largest lattice sizes that were considered in the minimization of the cost function Eq. (14). On the left, the data for the 2D ten-state Potts model are plotted with the parameters $\nu = 1.2594$ and $\theta_c = 1.457$. On the right, the data for the 3D ten-state Potts model are plotted with the parameters $\nu = 1.008$, $\theta_c = 2.332$.

docritical point $\bar{\theta}_c(L)$ as $|\bar{\theta}_c(L) - \theta_c| = aL^{-1/\nu_s}$, where θ_c, a, and ν_s are free parameters. The notation ν_s is used here to distinguish this estimate from that obtained from the collapse of the probability distribution. The average pseudocritical point is plotted in Fig. 3 for the 2D and 3D ten-state Potts models. For the other values of the number of states q that were considered ($q = 3, 5, 20$, and 50), the curves are similar. We tried to take into account possible algebraic scaling corrections by performing a nonlinear fit of the data with the function $|\bar{\theta}_c(L) - \theta_c| = aL^{-1/\nu_s}(1 + bL^{-\omega})$, where now θ_c, a, ν_s, b, and ω are free parameters. Due to the small number of degrees of freedom, this fit turned out to be quite unstable, different fitting algorithms leading to incompatible values. An indirect method was therefore applied to estimate the true exponent ν_s: the nonlinear fit $|\bar{\theta}_c(L) - \theta_c| = aL^{-1/\nu_s}$ was performed on various ranges of lattice sizes. A $L_{\min}$-dependent effective exponent $\nu_s(L_{\min})$ is then estimated by a nonlinear fit restricted to the lattice sizes $L \geqslant L_{\min}$. As can be seen in Fig. 4 for $q = 10$, this effective exponent is relatively stable for small $L_{\min}$ but displays large fluctuations at large $L_{\min}$

TABLE I. Estimates of the critical point θ_c and correlation length exponent ν of the 2D and 3D random Potts models. θ_c and ν were obtained by imposing the collapse of the probability distribution $P(u)$.

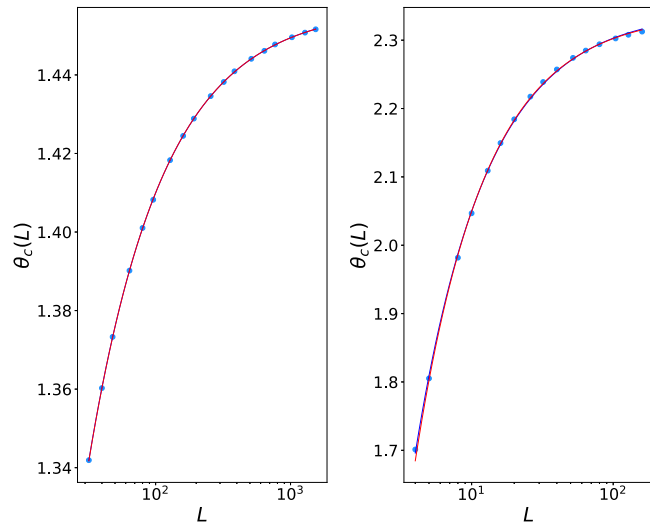| 2D	$q = 2$	3	5	10	20	50
θ_c	1.678(1)	1.563(1)	1.495(1)	1.457(1)	1.442(1)	1.435(1)
ν	1.25(2)	1.24(2)	1.25(2)	1.26(2)	1.24(2)	1.25(2)
3D	$q = 2$	3	5	10	20	50
θ_c	2.532(1)	2.420(1)	2.359(1)	2.332(1)	2.325(1)	2.327(1)
ν	1.01(1)	1.004(10)	1.001(10)	1.008(10)	1.004(10)	1.005(10)

FIG. 3. Average critical point $\bar{\theta}_c(L)$ vs the lattice size L of the 2D (left) and 3D (right) $q = 10$ Potts model. The blue curve corresponds to a simple fit without any correction, while the red curve corresponds to a fit with an algebraic correction. They can be distinguished on the figure for small L in the 3D case.

FIG. 5. Standard deviation of the critical point $\Delta\theta_c(L)$ vs the lattice size L of the 2D (left) and 3D (right) $q = 10$ Potts models. The blue curve is a linear fit.

because of a number of degrees of freedom of the fit becoming smaller and smaller. The error bars on $\nu_s(L_{\min})$ correspond to the standard deviation of the fit. They do not take into account the accuracy on $\theta_c(L)$, equal to 10^{-5}, which leads to a much smaller contribution [or order $\mathcal{O}(10^{-5})$] to the error on $\nu_s(L_{\min})$. In the 2D case, the effective exponents do not vary significantly with $L_{\min}$, which means that scaling corrections are weak. The exponents for different numbers of states q of the Potts model are compatible within error bars. In contrast, for the 3D Potts model, the influence of a correction is clearly
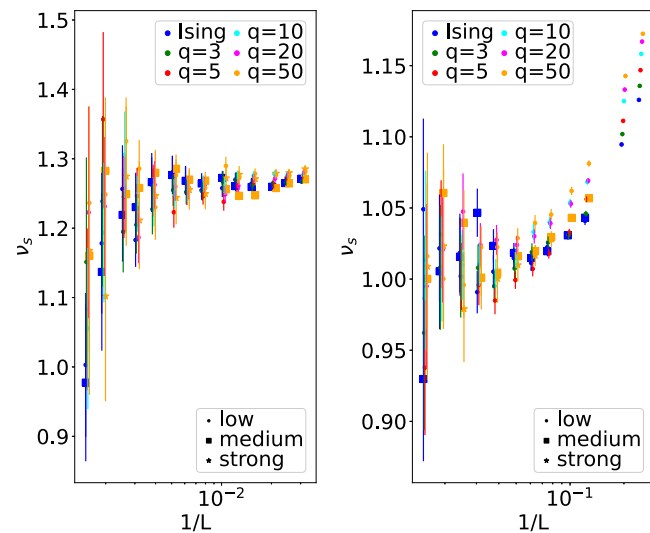

FIG. 4. Effective exponent ν_s vs the smallest lattice size $L_{\min}$ entering into the fit for the 2D (left) and 3D (right) Potts models. The different colors correspond to different numbers of states q of the Potts model. The different symbols correspond to different initial probability distributions of the couplings.
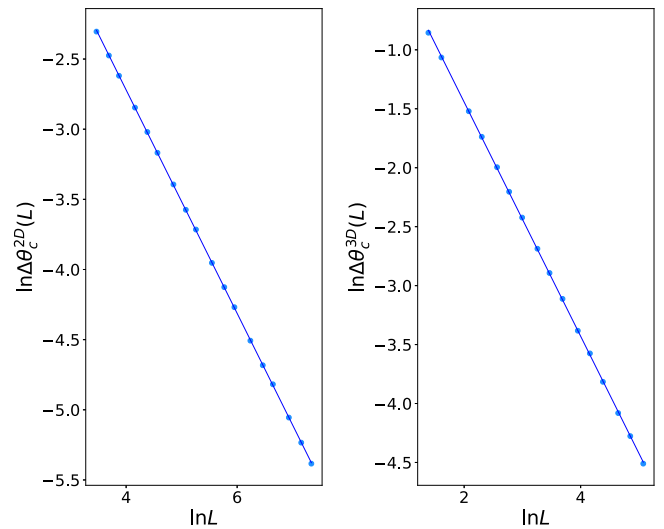
seen as a stronger dependence of the effective exponents on $1/L_{\min}$. For small $L_{\min}$, the exponents ν_s of the q-state Potts models increase with q and are fully incompatible. As $L_{\min}$ is increased, the exponents take smaller values and their dispersion shrinks, although their fluctuations increase. For large $L_{\min}$, a plateau seems to be reached at around $\nu_s \simeq 1.00$.

Finally, a third estimate of the correlation exponent ν was obtained from the standard deviation $\Delta\theta_c(L) = \sqrt{\overline{\theta_c^2(L)} - (\overline{\theta_c(L)})^2}$. The latter is expected to scale as $L^{-1/\nu}$ with the lattice size. A linear fit (in log-log scale) with only two free parameters is therefore sufficient in this case. To distinguish from the previous estimates, the exponent estimated from the standard deviation $\Delta\theta_c(L)$ will be denoted as ν_w in the following. An example for the 2D and 3D ten-state Potts model is presented in Fig. 5. The presence of scaling corrections is observed in the 3D case. Effective exponents $\nu_w(L_{\min})$, estimated by restricting the fit to lattice sizes $L \geqslant L_{\min}$, are shown on Fig. 6. In the 2D case, the effective exponents ν_w are spread around the value 1.25 for small $L_{\min}$, i.e., for fits over all or most of the lattice sizes, and are compatible within error bars. However, different evolutions are observed as $L_{\min}$ is increased. Some exponents increase while others decrease. Note that the effective exponents $\nu_w(L_{\min})$ for a given number of states q and a given initial distribution of the couplings are highly correlated because they were computed with fits over the same set of data. We were not able to identify a correlation between these different behaviors and the number of states q of the Potts model or the strength of disorder in the initial distribution of the couplings. These different evolutions at large $L_{\min}$ are therefore probably statistical fluctuations. The 3D case is hopefully a bit clearer. The effective exponents decrease with $L_{\min}$ and are compatible within error bars or close to the value $\nu_w \simeq 0.98$ in the limit $1/L_{\min} \to 0$. We have no reason to believe that different Potts models belong to a different universality class.

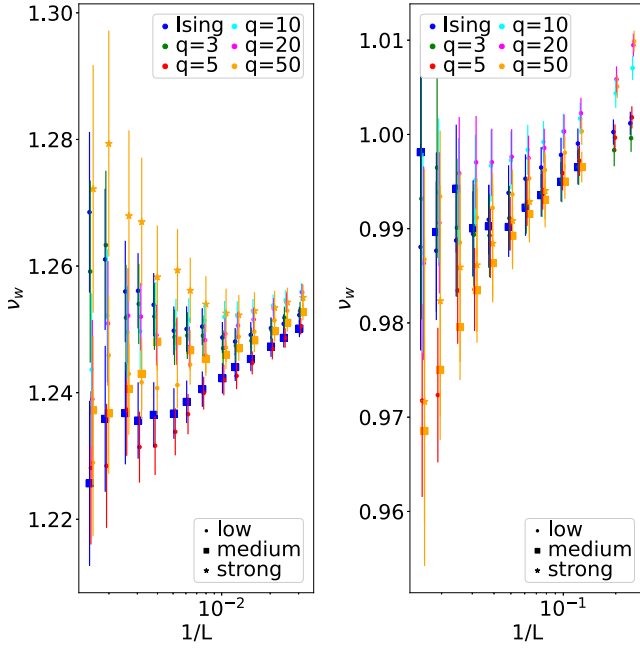FIG. 6. Effective exponent ν_w vs the smallest lattice size $L_{\min}$ entering into the fit for the 2D (left) and 3D (right) Potts models. The different colors correspond to different numbers of states q of the Potts model. The different symbols correspond to different initial probability distributions of the couplings.

FIG. 7. Average magnetic moment of the last decimated cluster $\bar{\mu}(L)$ vs the lattice size L of the 2D (left) and 3D (right) $q = 10$ Potts model. In the 3D case, the light-blue curve corresponds to a simple fit without any correction, while the red curve corresponds to a fit with an algebraic correction.

From the effective exponents at large $L_{\min}$, a rough estimate of the correlation lengths exponents can be inferred: $\nu_s \simeq 1.25(6)$ and $\nu_w \simeq 1.25(3)$ in the 2D case, and $\nu_s \simeq 1.01(5)$ and $\nu_w \simeq 0.985(10)$ in the 3D case. These estimates are compatible within error bars with the values of the literature for the Ising model: 1.24(2) in the 2D case [25] and $\nu_s = 0.99(2)$ and $\nu_w = 0.97(5)$ in the 3D case [26].

IV. MAGNETIC EXPONENT

The computation of the magnetic moment μ of the last decimated cluster has revealed unexpected difficulties: for a given sample, μ often displays a jump at the pseudocritical point. This jump is rare and quite small for the Ising model but more frequent and larger when the number of states q of the Potts model is increased. Since the pseudocritical points $\theta_c^i(L)$ of each sample are estimated with an accuracy of 10^{-5}, the estimates of the magnetic moment take randomly the value at the left or at the right of the jump. The average magnetic moment is therefore equal to the mean of the values at the left and at the right of the jump. We have checked that the relative width of this jump decreases with the lattice size L. For power-law initial distributions of the couplings (6), broader than the uniform ones, smaller jumps were observed.

The fractal dimension d_f of magnetization is estimated from the finite-size scaling

$$\bar{\mu} \sim L^{d_f} \tag{15}$$

of the average magnetic moment $\bar{\mu}$ of the last decimated cluster at the pseudocritical point $\theta_c^i(L)$ of each sample. Even though magnetization is a non-self-averaging quantity, as
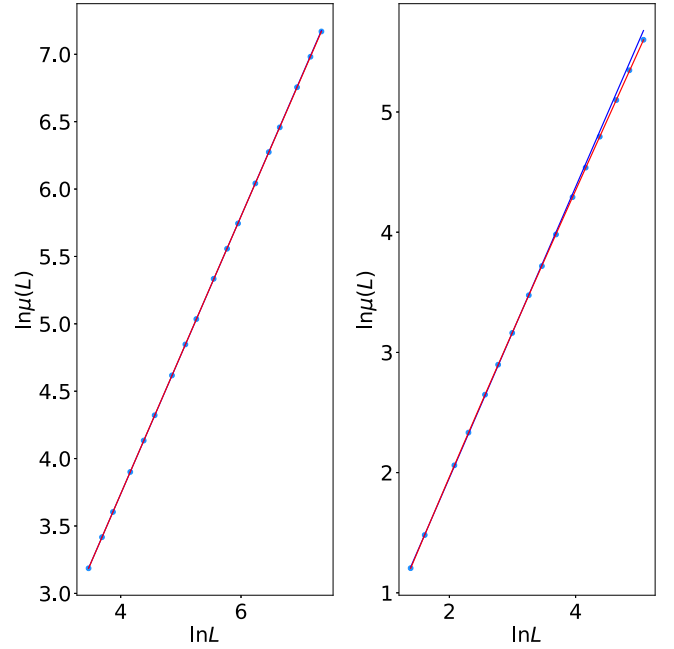
shown by a nonzero critical width $R_\mu = \frac{\overline{\mu^2} - \bar{\mu}^2}{\bar{\mu}^2}$ (in the range 0.12–0.13 for the 2D Potts model and 0.15–0.19 in 3D), the finite-size scaling Eq. (15) must be asymptotically satisfied by each sample, in contrast to the correlation length, which is a local quantity and whose average and typical values scale differently. Wiseman and Domany [38] have shown that it is a more efficient strategy to measure μ at $\theta_c^i(L)$ rather than at θ_c, because in the former case the sample-to-sample fluctuations are drastically reduced. The average magnetic moment $\bar{\mu}$ is plotted in Fig. 7 for the 2D and 3D ten-state Potts models. For the other values of the number of states q that were considered ($q = 3, 5, 20$, and 50), the curves are similar. The blue curve is the result of a linear fit of $\ln \bar{\mu}$ with $\ln L$. In both the 2D and 3D cases, the estimated fractal dimensions d_f are incompatible and systematically increase with the number of states q of the Potts model. A nonlinear fit with an algebraic correction, $\bar{\mu} = aL^{d_f}(1 + bL^{-\omega})$, was performed, but none of the algorithms that were used gave a stable estimate of d_f. To nevertheless take into account possible q-dependent scaling corrections, the fit was performed on various ranges of lattice sizes. As for the correlation length exponent, a $L_{\min}$-dependent effective exponent $d_f(L_{\min})$, is estimated by a fit restricted to the lattice sizes $L \geqslant L_{\min}$. This effective exponent is shown in Fig. 8. The influence of a correction is clearly seen as a dependence with $1/L_{\min}$. In the case of the 2D random Potts model, the fractal dimension d_f increases with $L_{\min}$ for the Ising model, is roughly stable for $q = 3$ and decreases for $q \geqslant 4$. As a consequence, the spreading of the effective exponents $d_f(L_{\min})$ decreases with $L_{\min}$. Even though all exponents are not compatible within error bars, the superuniversality of
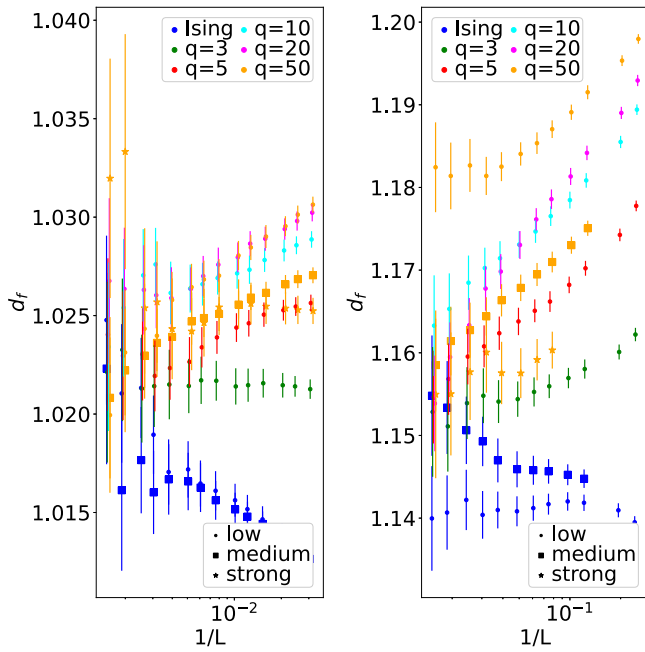
FIG. 8. Effective exponent d_f vs the smallest lattice size L_{min} entering into the fit for the 2D (left) and 3D (right) Potts models. The different colors correspond to different numbers of states q of the Potts model. The different symbols correspond to different initial probability distributions of the couplings.

FIG. 9. Average energy gap $\zeta = -\ln \overline{\Delta E}$ of the last decimated cluster vs the lattice size L of the 2D (left) and 3D (right) $q = 10$ Potts model. The curve is the nonlinear fit $-\ln \overline{\Delta E} = a + bL^\psi$.

the 2D random Potts models seems much more plausible than without taking into account scaling corrections. In the case of the 3D random Potts model, the scenario is similar. When scaling corrections are not taken into account, the estimates of the fractal dimensions d_f are fully incompatible. As L_{min} is increased, the spreading of the effective exponents $d_f(L_{min})$ shrinks and the fractal dimensions are finally compatible with the value 1.155. Two exceptions can be noticed: the Ising model and the $q = 50$ Potts model with weak disorder, whose exponents are still far from 1.155 at large L_{min}. However, at medium disorder, the exponents are remarkably closer to others and are compatible with 1.155 at large L_{min}.

From the effective exponents at large L_{min}, the fractal dimensions can be estimated to be $d_f \simeq 1.021(5)$ for the 2D random Potts model and 1.155(8) for the 3D model. These estimates are compatible within error bars with the values of the literature for the Ising model: 1.018(16) for the 2D Ising model [25] and 1.161(15) for the 3D Ising model [26].

V. ENERGY EXCITATION

At the IDFP, the largest energy scale Ω decreases as

$$\Omega \sim \Omega_0 e^{-cL^\psi} \quad \Leftrightarrow \quad \log \frac{\Omega}{\Omega_0} \sim -L^\psi \qquad (16)$$

during the SDRG flow. The same relation is expected to hold for the energy gap ΔE of the last decimated cluster, i.e., the smallest transverse field that was decimated in our implementation of the SDRG. On Fig. 9, the numerical data are presented for the ten-state 2D and 3D random Potts models. A nonlinear fit of $-\ln \overline{\Delta E} = a + bL^\psi$ is performed over the
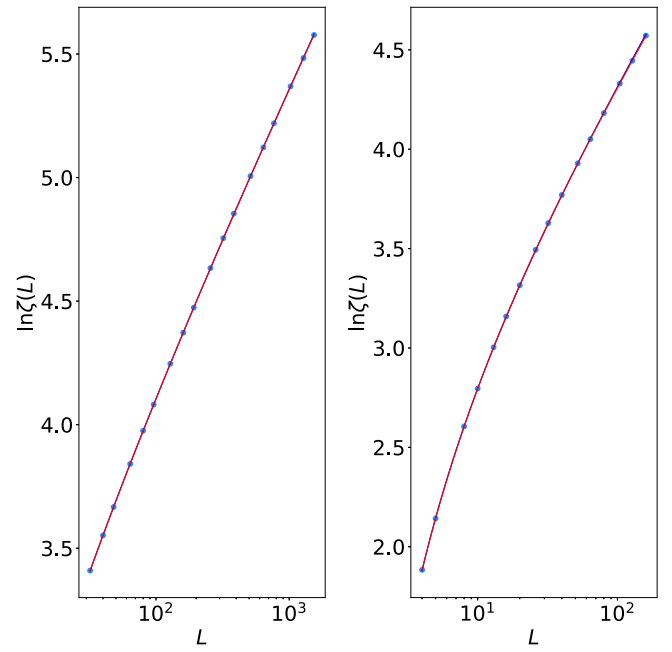
lattice sizes $L \geqslant L_{min}$ to estimate an effective critical exponent $\psi(L_{min})$. The latter is shown in Fig. 10. Note that there are three free parameters in this fit, so the accuracy will be smaller than for ν_w and d_f. In the 2D case, the effective exponents
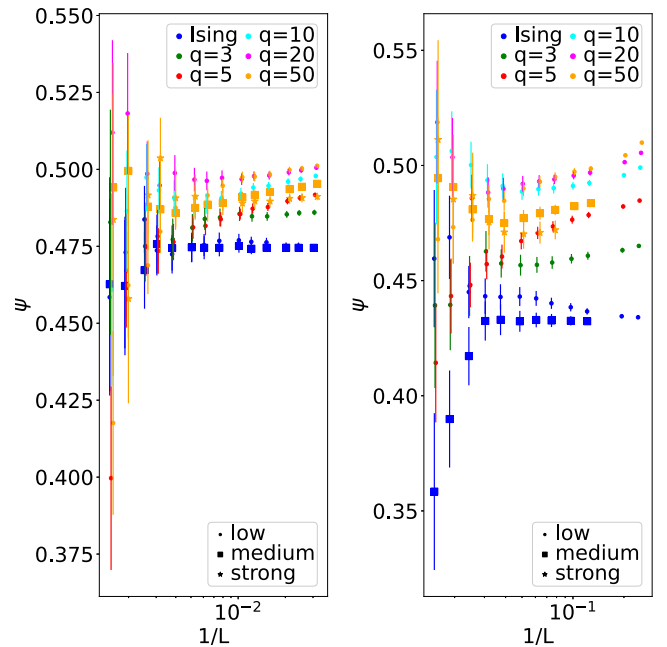

FIG. 10. Effective exponent ψ vs the smallest lattice size L_{min} entering into the fit for the 2D (left) and 3D (right) Potts models. The different colors correspond to different numbers of states q of the Potts model. The different symbols correspond to different initial probability distributions of the couplings.

$\psi(L_{\min})$ are incompatible and increase with the number of states q of the Potts model for small $L_{\min}$. However, for large $L_{\min}$, the q dependence becomes smaller and the exponents are finally compatible within error bars with the value 0.485. In the 3D case, the exponents ψ are also incompatible and increase with the number of states q of the Potts model at small $L_{\min}$. As in the 2D case, the spreading shrinks at large $L_{\min}$ but not enough for the exponents to become compatible with error bars. Larger lattices sizes would be helpful to reach a definitive conclusion.

From the effective exponents at large $L_{\min}$, the exponent ψ can be estimated to $\psi \simeq 0.48(2)$ for the 2D random Potts model and 0.46(4) for the 3D model. These estimates are compatible within error bars with the values of the literature for the Ising model: 0.46(2) for the 2D Ising model [25] and 0.48(2) for the 3D Ising model [26].

VI. CONCLUSIONS

When scaling corrections are not taken into account, the critical exponents d_f and ψ were shown to take, both in 2D and 3D, incompatible values that increase with the number of states q of the Potts model. Since nonlinear fits involving algebraic scaling corrections are unstable, effective exponents were estimated over shrinking ranges of lattice sizes $L \geqslant L_{\min}$. The limit $1/L_{\min} \to 0$ of these effective exponents is expected to give the critical exponent at the IDFP. The analysis is, however, hampered by the large fluctuations of the effective exponents due to the smaller number of degrees of freedom in the fit at large $L_{\min}$. Nevertheless, scaling corrections are clearly observed. While the latter do not seem to depend on q for the correlation length exponent (apart from ν_s in the 3D case), the corrections on the magnetic fractal dimension d_f are

TABLE II. Summary of the estimates of the critical exponents of the 2D and 3D random Potts models.

	ν_s	ν_w	d_f	ψ
2D	1.25(6)	1.25(3)	1.021(5)	0.48(2)
3D	1.01(5)	0.985(10)	1.155(8)	0.46(4)

strongly q dependent. A shrinking of the dispersion of the effective exponents for different numbers of states q is observed when $L_{\min}$ is increased, providing evidence of the existence of a superuniversality class. This conclusion is in agreement with Ref. [30], where the superuniversality of the 2D random Potts model is shown by means of a mapping onto a lattice gauge model. The effective exponents ψ display a behavior similar to d_f, although less pronounced and with a residual dispersion of the exponents in the limit $1/L_{\min} \to 0$. Our final estimates of the critical exponents at the IDFP are summarized in Table II. As noticed in the text, they are compatible with previous estimates obtained for the Ising model.

The question of the extension of the random quantum Ising universality class naturally arises. The 1D case was discussed in the Introduction. In dimensions $d \geqslant 2$, it is not known whether the Ashkin-Teller model or the clock model also belong to the Ising universality class. These are some of the open questions that we will try to address in the future.

[1] C. Dasgupta and S. Ma, Low-temperature properties of the random Heisenberg antiferromagnetic chain, Phys. Rev. B **22**, 1305 (1980).

[2] D. S. Fisher, Random Transverse Field Ising Spin Chains, Phys. Rev. Lett. **69**, 534 (1992).

[3] D. S. Fisher, Critical behavior of random transverse-field Ising spin chains, Phys. Rev. B **51**, 6411 (1995).

[4] F. Iglói and C. Monthus, Strong disorder RG approach of random systems, Phys. Rep. **412**, 277 (2005).

[5] F. Iglói and C. Monthus, Strong disorder RG approach–A short review of recent developments, Eur. Phys. J. B **91**, 290 (2018).

[6] T. Vojta, Rare region effects at classical, quantum and nonequilibrium phase transitions, J. Phys. A: Math. Gen. **39**, R143 (2006).

[7] F. Iglói, Exact renormalization of the random transverse-field Ising spin chain in the strongly ordered and strongly disordered Griffiths phases, Phys. Rev. B **65**, 064416 (2002).

[8] T. Senthil and S. N. Majumdar, Critical Properties of Random Quantum Potts and Clock Models, Phys. Rev. Lett. **76**, 3001 (1996).

[9] J. Cardy and J. L. Jacobsen, Critical Behavior of Random-Bond Potts Models, Phys. Rev. Lett. **79**, 4063 (1997).

[10] C. Chatelain and B. Berche, Finite-Size Scaling Study of the Surface and Bulk Critical Behavior in the Random-Bond Eight-State Potts Model, Phys. Rev. Lett. **80**, 1670 (1998).

[11] J. L. Jacobsen and J. Cardy, Critical behaviour of random-bond Potts models: A transfer matrix study, Nucl. Phys. B **515**, 701 (1998).

[12] C. Chatelain and B. Berche, Universality and multifractal behaviour of spin-spin correlation functions in disordered Potts models, Nucl. Phys. B **572**, 626 (2000).

[13] E. Carlon, P. Lajkó, and F. Iglói, Disorder Induced Cross-Over Effects at Quantum Critical Points, Phys. Rev. Lett. **87**, 277201 (2001).

[14] J. Hooyberghs, F. Iglói, and C. Vanderzande, Strong Disorder Fixed Point in Absorbing-State Phase Transitions, Phys. Rev. Lett. **90**, 100601 (2003).

[15] J. Hooyberghs, F. Iglói, and C. Vanderzande, Absorbing state phase transitions with quenched disorder, Phys. Rev. E **69**, 066140 (2004).

[16] T. Vojta and M. Dickison, Critical behavior and Griffiths effects in the disordered contact process, Phys. Rev. E **72**, 036126 (2005).

[17] P. Goswami, D. Schwab, and S. Chakravarty, Rounding by Disorder of First-Order Quantum Phase Transitions: Emergence of Quantum Critical Points, Phys. Rev. Lett. **100**, 015703 (2008).

[18] F. Hrahsheh, J. A. Hoyos, R. Narayanan, and T. Vojta, Strong-randomness infinite-coupling phase in a random quantum spin chain, Phys. Rev. B **89**, 014401 (2014).

[19] C. Chatelain and D. Voliotis, Numerical evidence of the double-Griffiths phase of the random quantum Ashkin-Teller chain, Eur. Phys. J. B **89**, 18 (2016).

[20] F. Hrahsheh, J. A. Hoyos, and T. Vojta, Rounding of a first-order quantum phase transition to a strong-coupling critical point, Phys. Rev. B **86**, 214204 (2012).

[21] H. Barghathi, F. Hrahsheh, J. A. Hoyos, R. Narayanan, and T. Vojta, Strong-randomness phenomena in quantum Ashkin–Teller models, Phys. Scr. T **165**, 014040 (2015).

[22] A. K. Ibrahim and T. Vojta, Monte Carlo simulations of the disordered three-color quantum Ashkin-Teller chain, Phys. Rev. B **95**, 054403 (2017).

[23] C. Chatelain, Improved matrix product operator renormalization group: Application to the N-color random Ashkin–Teller chain, J. Stat. Mech. (2019) 093301.

[24] O. Motrunich, S.-C. Mau, D. A. Huse, and D. S. Fisher, Infinite-randomness quantum Ising critical fixed points, Phys. Rev. B **61**, 1160 (2000).

[25] I. A. Kovács and F. Iglói, Renormalization group study of the two-dimensional random transverse-field Ising model, Phys. Rev. B **82**, 054437 (2010).

[26] I. A. Kovács and F. Iglói, Infinite-disorder scaling of random quantum magnets in three and higher dimensions, Phys. Rev. B **83**, 174207 (2011).

[27] I. A. Kovács and F. Iglói, Renormalization group study of random quantum magnets, J. Phys.: Condens. Matter **23**, 404204 (2011).

[28] U. Agrawal, S. Gopalakrishnan, and R. Vasseur, Universality and quantum criticality in quasiperiodic spin chains, Nat. Commun. **11**, 2225 (2020).

[29] U. Agrawal, S. Gopalakrishnan, and R. Vasseur, Quantum Criticality in the 2D Quasiperiodic Potts Model, Phys. Rev. Lett. **125**, 265702 (2020).

[30] B. Kang, S. A. Parameswaran, A. C. Potter, R. Vasseur, and S. Gazit, Superuniversality from disorder at two-dimensional topological phase transitions, Phys. Rev. B **102**, 224204 (2020).

[31] M. J. Stephen and L. Mittag, Pseudo-Hamiltonians for the Potts model at the critical point, Phys. Lett. A **41**, 357 (1972).

[32] J. Sólyom and P. Pfeuty, Renormalization-group study of the Hamiltonian version of the Potts model, Phys. Rev. B **24**, 218 (1981).

[33] R. L. Greenblatt, M. Aizenman, and J. L. Lebowitz, Rounding of First Order Transitions in Low-Dimensional Quantum Systems with Quenched Disorder, Phys. Rev. Lett. **103**, 197201 (2009).

[34] M. Aizenman, R. L. Greenblatt, and J. L. Lebowitz, Proof of rounding by quenched disorder of first order transitions in low-dimensional quantum systems, J. Math. Phys. **53**, 023301 (2012).

[35] C. Chatelain, B. Berche, W. Janke, and P. E. Berche, Softening of first-order transition in three-dimensions by quenched disorder, Phys. Rev. E **64**, 036120 (2001).

[36] C. Chatelain, B. Berche, W. Janke, and P.-E. Berche, Monte Carlo study of phase transitions in the bond-diluted 3D 4-state Potts model, Nucl. Phys. B **719**, 275 (2005).

[37] T. H. Cormen, C. E. Leiserson, R. L. Rivest, and C. Stein, *Introduction to Algorithms* (MIT Press and McGraw-Hill, 2001).

[38] S. Wiseman and E. Domany, Self-averaging, distribution of pseudocritical temperatures, and finite size scaling in critical disordered systems, Phys. Rev. E **58**, 2938 (1998).